IOPscience iopscience.iop.org

Home Search Collections Journals About Contact us My IOPscience

Numerical investigation of a tunable band-pass plasmonic filter with a hollow-core ring resonator

This content has been downloaded from IOPscience. Please scroll down to see the full text.

2011 J. Opt. 13 035004

(http://iopscience.iop.org/2040-8986/13/3/035004)

View the table of contents for this issue, or go to the journal homepage for more

Download details:

IP Address: 115.156.166.115
This content was downloaded on 25/12/2014 at 07:45

Please note that terms and conditions apply.

IOP Publishing Journal of Optics

J. Opt. **13** (2011) 035004 (7pp) doi:10.1088/2040-8978/13/3/035004

Numerical investigation of a tunable band-pass plasmonic filter with a hollow-core ring resonator

Amir Setayesh[1], **S Reza Mirnaziry and Mohammad Sadegh Abrishamian**

Department of Electrical Engineering, K N Toosi University of Technology, PO Box 16315-1355, Tehran, Iran

E-mail: setayesh_a@ee.kntu.ac.ir, S.R.MIRNAZIRY@ee.kntu.ac.ir and msabrish@eetd.kntu.ac.ir

Received 18 November 2010, accepted for publication 21 January 2011
Published 24 February 2011
Online at stacks.iop.org/JOpt/13/035004

Abstract

In this study, a compact nanoscale plasmonic filter which consists of two metal–insulator–metal (MIM) waveguides coupled to each other by a rectangular ring resonator is presented and investigated numerically. The propagating modes of surface plasmon polaritons (SPPs) are studied in this structure. By replacing a portion of the ring core with air, while the outer dimensions of the structure are kept constant, we illustrate the possibility of the redshift of resonant wavelengths in order to tune the resonance modes. This feature is useful for integrated circuits in which we have limitations on the outer dimensions of the filter structure and it is not possible to enlarge the dimension of the ring resonator to reach longer resonant wavelengths. The corresponding results are illustrated by the 2D finite-difference time-domain (FDTD) method. The proposed structure has potential applications in plasmonic integrated circuits and can be simply fabricated.

Keywords: plasmonics, surface plasmon polaritons, MIM waveguide, plasmonic filter, ring resonator

(Some figures in this article are in colour only in the electronic version)

1. Introduction

During recent years, plasmonics has been presented as a future technology in integrated circuits incorporating the compactness of electronics and the wide bandwidth created by current optical networks [1]. In the region of integrated optics, plasmonic waveguides act as components to guide optical signals to different parts of the circuits. The capability of confining light beyond the diffraction limit and the ability to fabricate devices with dimensions bellow 100 nm, has promised an evolution in optoelectronic circuits [2]. To guide plasmonic waves, different geometries have been proposed such as Mach–Zehnder interferometers [3], splitters [4], plasmon Bragg reflectors [5], Bragg gratings with periodically varied width [6, 7], metal–insulator–metal waveguides [8, 9], nanowires [10, 11], chains of nanoparticles [12–14], grooves and wedges [15, 16], etc. Although some of these nanoguides are inconvenient to implement in optical circuits, MIM waveguides have attracted considerable attention due to their simplicity in fabrication and strong field confinement [17].

During recent years, some simple structures have been proposed for plasmonic filters, such as channel drop filters with disc resonators [18], rectangular geometry resonators [19, 20] and ring resonators [18, 21]. In comparison with the complex structures of Bragg reflectors, the mentioned structures can be fabricated much more easily. Two typical types of plasmonic filters in MIM waveguides are band-pass and band-stop filters. In band-stop filters, the majority of the input light spectrum is allowed to pass through the filter and only several wavelengths are prohibited from propagation in the structure. But the band-pass filters are in contrast to band-stop filters, i.e. they let just

[1] Author to whom any correspondence should be addressed.

 © 2011 IOP Publishing Ltd Printed in the UK & the USA

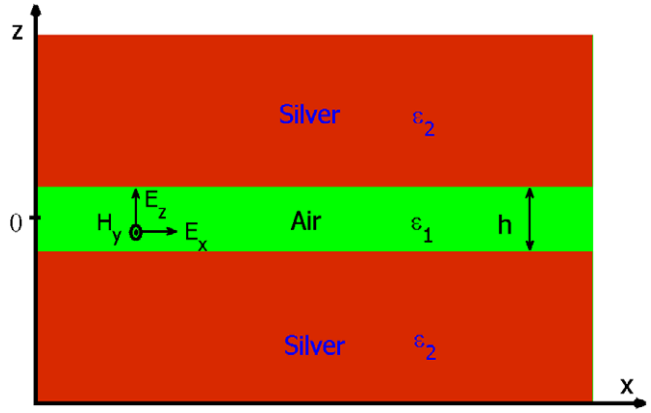

Figure 1. Schematic of an MIM structure with two semi-infinite metal slabs of permittivity ε_2 surrounding a dielectric layer of thickness h and permittivity ε_1.

some specific wavelengths pass through them and reject the majority of the input light spectrum.

One of the most interesting features of filters is to have tunable resonance wavelengths. In previous works, by varying the outer dimensions of the structure, i.e. cavity length or radius, tunable filters were achieved [21–23]. Here, we want to hollow out the core of a rectangular ring resonator—while leaving the outer size of the structure constant—in order to achieve a redshift in resonant wavelengths of the filter. As we know, according to some significant limitations on the circuit components' dimensions, it may not be possible to enlarge the size of the ring resonator to reach longer resonant wavelengths. Therefore the new method is beneficial in miniaturizing the filters in the case of integrated circuits. The transmittance characteristics of the proposed filter are presented by the 2D FDTD method. This study is as follows. In section 2, the fundamental propagation mode of MIM structures is reviewed. In section 3, first a simple plasmonic filter with a rectangular ring resonator is investigated and then, to reach a tunable band-pass filter, a hollow-core ring resonator is introduced and investigated numerically. Then we look for a way to overcome the decrease of the transmittance peak. Finally, section 4 concludes the paper.

2. Dispersion relation and effective refractive index of an MIM waveguide

In this section, the MIM structure and relations between the components of the propagating field inside them are reviewed. Consider an MIM waveguide composed of two semi-infinite metal slabs surrounding a dielectric layer of thickness h (see figure 1). Each metal–dielectric interface located on two sides of the MIM waveguide supports localized transverse magnetic (TM) SPP modes propagating along the x direction. It would be anticipated that, when the space between the two interfaces is comparable to the decay lengths of SPPs in the dielectric, the SPP modes become coupled to each other [24].The field components inside the dielectric layer can be calculated using

Table 1. Parameters of the Drude–Lorentz model for silver [27].

n	ω_n (eV)	Γ_n (eV)	f_n
1	0.816	3.886	0.065
2	4.481	0.452	0.124
3	8.185	0.065	0.011
4	9.083	0.916	0.840
5	20.29	2.419	5.646

the Maxwell relations ($\exp(+\mathrm{i}\omega t)$ time convention is assumed and suppressed)

$$E_x = -\mathrm{i}A\frac{1}{\omega\varepsilon_0\varepsilon_1}k_1\mathrm{e}^{\mathrm{i}\beta x}\mathrm{e}^{k_1 z} + \mathrm{i}B\frac{1}{\omega\varepsilon_0\varepsilon_1}k_1\mathrm{e}^{\mathrm{i}\beta x}\mathrm{e}^{-k_1 z} \quad (1a)$$

$$E_z = A\frac{\beta}{\omega\varepsilon_0\varepsilon_1}\mathrm{e}^{\mathrm{i}\beta x}\mathrm{e}^{k_1 z} + B\frac{\beta}{\omega\varepsilon_0\varepsilon_1}\mathrm{e}^{\mathrm{i}\beta x}\mathrm{e}^{-k_1 z} \quad (1b)$$

$$H_y = A\mathrm{e}^{\mathrm{i}\beta x}\mathrm{e}^{k_1 z} + B\mathrm{e}^{\mathrm{i}\beta x}\mathrm{e}^{-k_1 z} \quad (1c)$$

where β is the propagation constant of the MIM waveguide which has a complex value and $k_1 = \sqrt{\beta^2 - k_0^2}$ is the wavevector perpendicular to the propagation direction (k_0 is the propagation constant of free space). For $h \ll \lambda$, among different modes which can be supported by MIM, only the first odd mode ($E_x(z)$ is an odd function, while $H_y(z)$ and $E_z(z)$ are even (see figure 1)) can propagate in the waveguide. The corresponding propagation constant β, can be attained from the following dispersion relation [25, 26]:

$$\tanh\left(\frac{k_1 h}{2}\right) = -\left(\frac{k_2\varepsilon_1}{k_1\varepsilon_2}\right). \quad (2)$$

Indices 1 and 2 are pointing to the dielectric layer and metal slabs, respectively. In this study, the metal sides of the MIM waveguide are assumed to be silver and the dielectric layer is considered to be air. As a reasonablely accurate model in the wavelength range from 0.2 to 2 μm, the seven-pole Drude–Lorentz model is employed to characterize the dielectric constant of metal. The fitting model is described as [27]

$$\varepsilon_1(\omega) = 1 - \frac{\omega_\mathrm{p}^2}{\omega(\omega - \mathrm{i}\gamma)} + \sum_{n=1}^{5}\frac{f_n\omega_n^2}{\omega_n^2 - \omega^2 + \mathrm{i}\omega\gamma_n} \quad (3)$$

where $\omega_\mathrm{p} = 2002.6$ THz is the bulk plasma frequency and $\gamma = 11.5907$ THz is the damping constant. The quantities of resonant frequencies ω_n, damping constants γ_n and weights f_n are given in table 1 [27].

We have calculated the effective refraction index ($n_\mathrm{eff} = \beta/k_0$) for different widths of MIM waveguides, using the IMSL Fortran subroutine. Figure 2 shows the calculated $\mathrm{Re}[n_\mathrm{eff}]$ and L_SPP (propagation length of SPPs defined as $L_\mathrm{SPP} = 1/(2\,\mathrm{Im}[\beta])$), as a function of wavelength.

For homogeneous structures, the coefficients of field components in equation (1) would be equal, i.e. $A = B$. So, the component E_x compared to E_z will be

$$\left|\frac{E_x}{E_z}\right| = \left|\frac{k_1}{\beta}\right|\tanh(k_1 z). \quad (4)$$

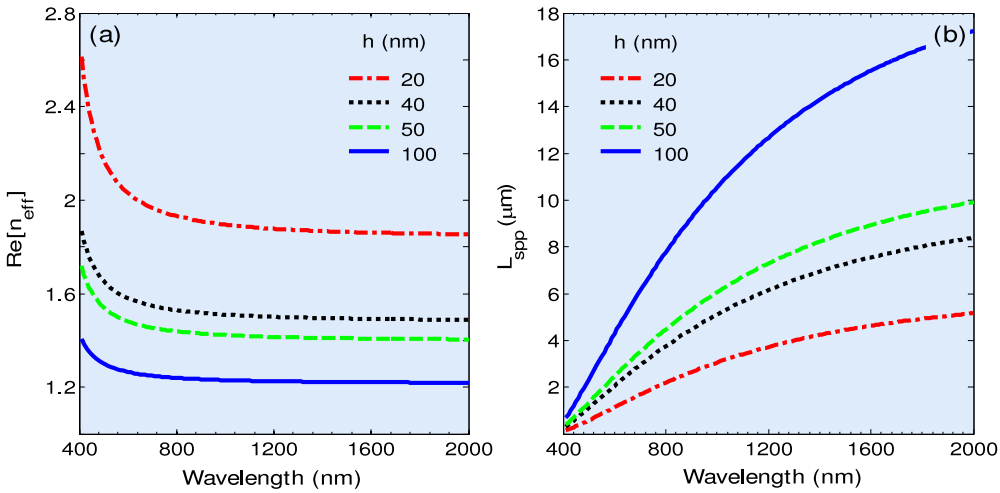

Figure 2. (a) Real part of the effective refraction index as a function of wavelength for different widths of the air layer in the Ag–air–Ag waveguide. (b) The corresponding propagation length of SPPs as a function of wavelength for the same widths.

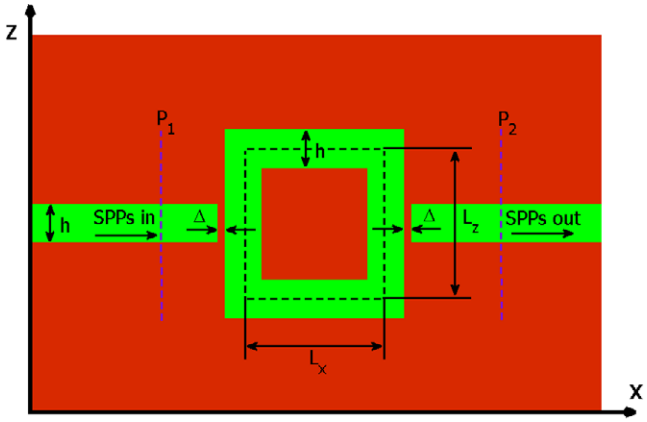

Figure 3. Schematic of a simple plasmonic filter consisting of two MIM waveguides coupled to each other by a rectangular ring resonator. h is set to 50 nm.

For an MIM waveguide with $h \ll \lambda$, this ratio is negligible, so we can ignore the longitudinal component and assume that the propagated mode in the MIM is similar to the TEM mode.

3. Plasmonic filter with a rectangular ring resonator

3.1. Simple waveguide filter with a rectangular ring resonator

Figure 3 shows the structure of a simple plasmonic filter which consists of two MIM waveguides coupled to each other by a rectangular ring resonator, first proposed in [22]. The filter parameters h, Δ, L_x and L_z are the width of the MIM, the gap distance between input/output MIM waveguides and the rectangular ring resonator, and corresponding side lengths of the rectangular ring resonator, respectively. To support only the TM mode in the MIM waveguide we set $h = 50$ nm, which is much smaller than the operating wavelengths.

Two power monitors are set at points P_1 and P_2 to detect the incident power A_1 (without the rectangular ring resonator) and the transmitted power A_2 (with the rectangular ring resonator). So, the power transmittance is $T = A_2/A_1$ [21, 27]. The transmittance of the filter with $L_x = L_z = 200$ nm and $\Delta = 10$ nm is shown in figure 2(a). One can see in figure 2(a) that there are two resonance peaks at $\lambda_1 \approx 1113$ nm and $\lambda_2 \approx 541.5$ nm. The length of the MIM waveguide in the ring cavity (cavity length) is the average length of the inner and outer perimeter, $L = 2(L_x + L_z) = 800$ nm, as illustrated by the dashed line in figure 3 [20, 22]. The condition of resonance for the rectangular ring cavity is [20, 21]

$$L = N\lambda_{\text{spp}} = N(\lambda/\operatorname{Re}[n_{\text{eff}}]), \qquad N = 1, 2, 3, \ldots. \quad (5)$$

As shown in figure 2(a), the $\operatorname{Re}[n_{\text{eff}}]$ of the MIM waveguides at $\lambda_1 = 1113$ nm and $\lambda_2 = 541.5$ nm are approximately 1.4 and 1.47, respectively. According to equation (5), the analytical resonance length for the first resonance is $L_{\text{res1}} \approx 795$ nm, which is approximately equal to the actual cavity length $L = 800$ nm, while $L_{\text{res2}} \approx 740$ nm for the second resonance has experienced a shift relative to the actual cavity length $L = 800$ nm. The transmittance of the simple plasmonic filter is calculated by 2D FDTD and is depicted in figure 4(a). Figures 4(b) and (c) show the field profile of $|E_z|$ for the first and second resonances of the filter, respectively. In the following FDTD simulations, the size of the uniform Yee cells in the x and z directions are set to be $\Delta x = \Delta z = 1$ nm and the computational space is surrounded by a convolutional perfectly matched layer (CPML) absorbing boundary.

3.2. Plasmonic filter with a hollow-core ring resonator

In this section, we investigate the effect of hollowing out the core of the ring resonator on resonance wavelengths of the filter while keeping its outer dimensions constant, i.e. L_x, L_z and Δ are kept constant. The proposed structure is depicted in figure 5. From the figure one can see that the core of the ring resonator is emptied with the widths of W_z and W_x.

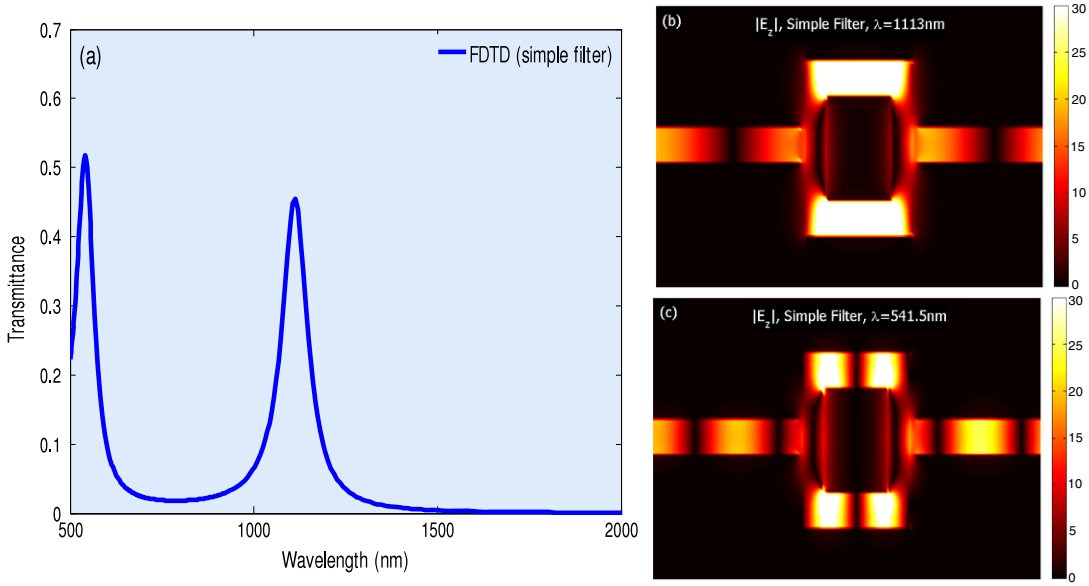

Figure 4. (a) The transmittance spectrum of the simple plasmonic filter with a square ring resonator ($L_x = L_z = 200$ nm, $\Delta = 10$ nm). (b) The $|E_z|$ field pattern of the simple plasmonic filter with a rectangular resonator at the first resonance wavelength equal to 1113 nm. (c) The $|E_z|$ field pattern of the filter at the second resonance wavelength equal to 541.5 nm.

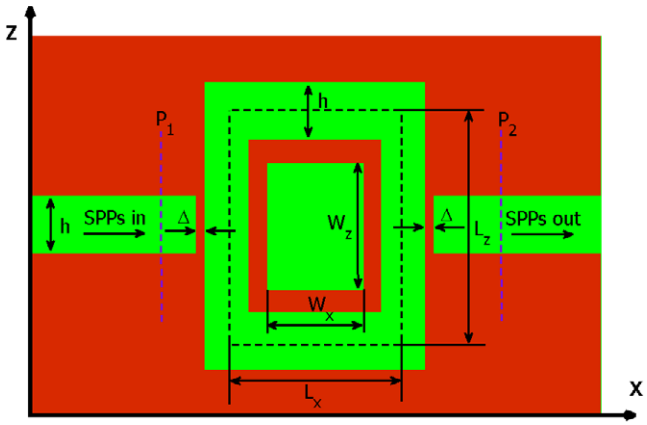

Figure 5. Schematic of a plasmonic filter with a rectangular hollow-core ring resonator. $h = 50$ nm, $L_x = L_z = 200$ nm, $\Delta = 10$ nm. W_z and W_x are variables.

At first we investigate the case $W_z = W_x$. The transmittance spectra of the proposed structure are calculated by FDTD and illustrated in figure 6(a). It can be seen that by varying W_z and W_x from 100 to 130 nm, the whole of the transmission spectrum experiences a redshift (so the third resonance mode is now observable in the window). Figure 6(b) shows that the wavelength shifts of the resonant modes 1 and 2 have approximately linear relations with the variation of hollow dimensions. This result is in accordance with the physical fact that, by increasing the area of resonance inside the ring, the resonant wavelength will be increased. According to the transmission curves illustrated in figure 6(a), it is clear that the band-pass filter can be easily tuned by adjusting the dimensions of the hollow.

Another possible case for the hollow-core ring resonator structure is to vary just one dimension of the hollow while keeping the other one constant, i.e. varying W_z while W_x is

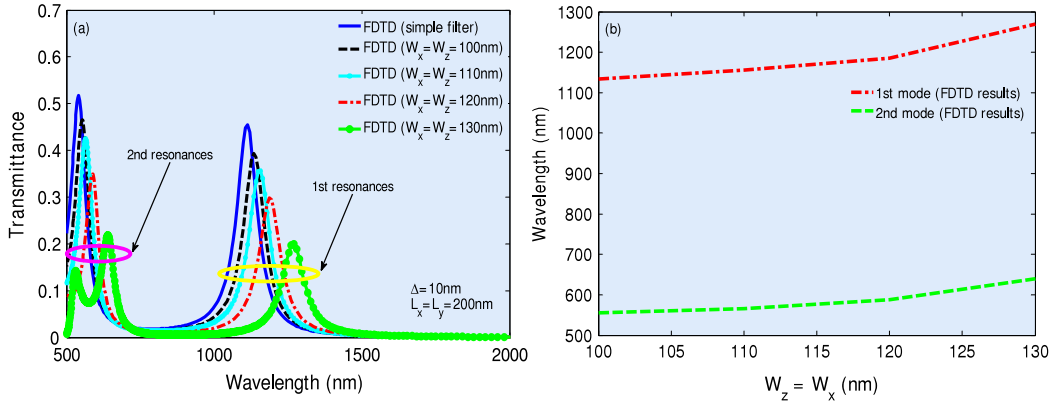

Figure 6. (a) Transmission spectra of the hollow-core ring resonator filter shown in figure 5 for different values of W_x and W_z (in this case of $W_x = W_z$). The resonance wavelengths have a redshift with increasing hollow dimensions. (b) Relationship between resonance wavelengths and hollow dimensions.

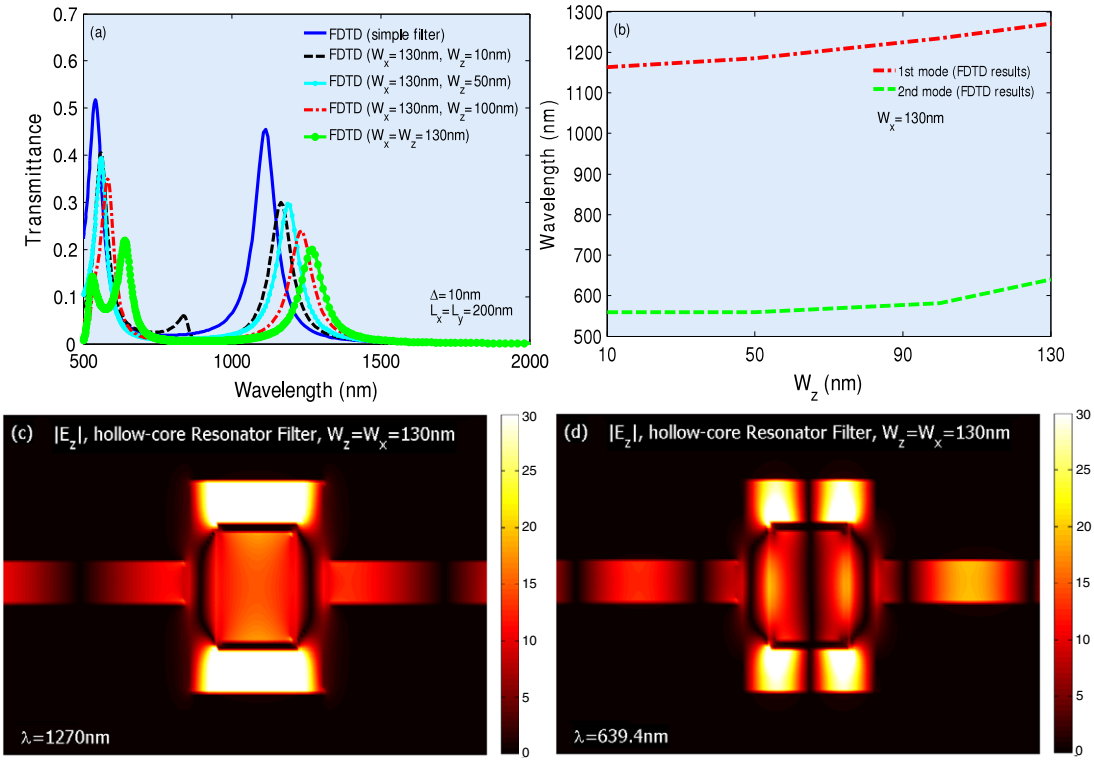

Figure 7. (a) Transmission spectra of the hollow-core ring resonator filter shown in figure 5 for different values of W_z (in this case: $W_x = 130$ nm is set to be constant but W_z is varied as is depicted in the figure). The resonance wavelengths have a redshift with increasing W_z. (b) Relationship between resonance wavelengths and W_z. (c) The $|E_z|$ field patterns of the filter at the first resonance wavelength of 1270 nm, for $W_x = W_z = 130$ nm. (c) The $|E_z|$ field patterns of the filter at the second resonance wavelength of 639.4 nm, for $W_x = W_z = 130$ nm.

kept constant (130 nm). The transmittance spectrum in this case is depicted in figure 7. Again, a redshift is observed in the resonance wavelengths but in a different manner in comparison with the previous case. Figure 7(b) shows that the wavelength shift of the first and second resonant modes has an approximately linear relation with the variation of W_z. Although we assumed $W_x = 130$ nm the same trend is expected for other values of W_x while W_z is varied. Figures 7(c) and (d) show the field profile of $|E_z|$ for the first and second resonances of the hollow-core ring resonator filter when $W_x = W_z = 130$ nm, respectively.

Although the redshift phenomenon can occur by altering the radius of the ring, as studied in previous works, they did not have any considerations about the structure size, whereas our discussions result in filter miniaturization. For instance, to have a filter with the first resonance at $\lambda_1 = 1270$ nm, we should have a simple conventional band-pass filter with $L_x = L_z = 225$ nm, but in the case of a hollow-core filter by setting $L_x = L_z = 200$ nm and hollowing out the core $W_x = W_z = 130$ nm, we can reach the same wavelength. This size reduction of about 12.5% for each side length is considerable.

3.3. Enhancing the transmittance peak

It is seen from figures 6(a) and 7(a) that, by increasing the dimensions of the hollow (and so shifting the resonance wavelength), the maximum of transmittance declines. To overcome this problem, we decrease the width of the ring

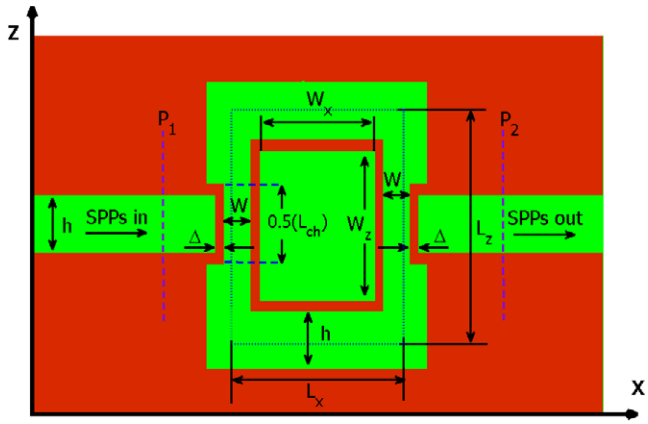

Figure 8. Schematic of the plasmonic filter with a rectangular hollow-core ring resonator and reduced width of the ring MIM waveguide at the coupling region. $h = 50$ nm, $L_x = L_z = 200$ nm, $\Delta = 10$ nm. W is variable.

MIM waveguide in the coupling region. The proposed structure is depicted in figure 8. The procedure of the transmittance increment of the first and second resonance modes of the structure is illustrated in figure 9(a). As can be seen from this figure by decreasing W, the coupling area between input/output MIM and ring MIM waveguides increases and therefore a greater amount of power will be coupled. Figure 9(a) reveals that the first resonance wavelength experiences no shifting by varying W, but the second mode

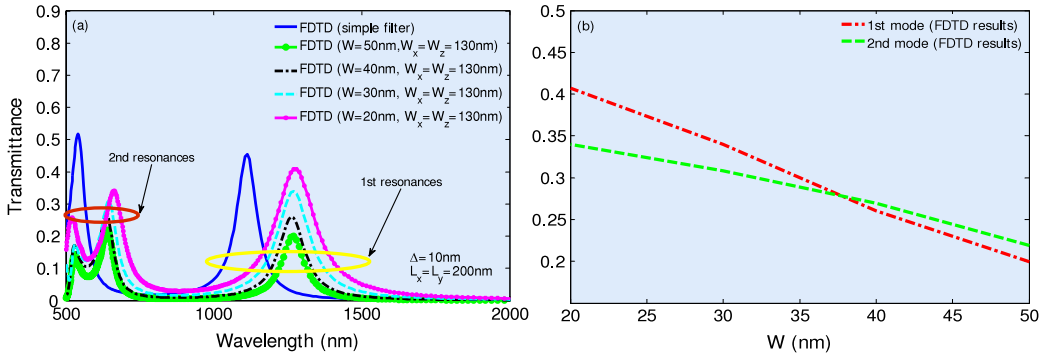

Figure 9. (a) Transmission spectra of the structure shown in figure 8, for $W_x = W_z = 130$ nm and different values of W. (b) Relationship between the transmittance of resonance wavelengths and W ($W_x = W_z = 130$ nm).

has a slight redshifting with respect to decreasing W. We believe that, since by decreasing W in the coupling regions their Re[n_{eff}] increases, this phenomenon can be observed (see figure 2(a)). By considering the resonant relation of a simple band-pass filter $L = \lambda/\text{Re}[n_{\text{eff}}]$, it is obvious that for a constant L by increasing Re[n_{eff}] the λ should also increase. Since $L_{\text{ch}} = 120$ nm (L_{ch} is the length of the ring MIM waveguide in the coupling regions) is much smaller in comparison with the first resonance ($\lambda_1 \approx 11L_{\text{ch}}$), we expect that the first resonance does not sense a significant change inside the ring and so is not shifted. But it is not the case for the second resonance. Since $\lambda_2 \approx 5L_{\text{ch}}$ is not much larger than L_{ch}, it senses a stronger change inside the ring; so it has experienced a slight redshift. The relation between decreasing W and the increase of transmittance for the first and second modes is illustrated in figure 9(b).

4. Conclusion

In this paper, a simple compact plasmonic filter based on MIM waveguides with a rectangular hollow-core ring resonator was proposed. To make the proposed filter tunable, a simple way of emptying the core of the ring was introduced and investigated numerically. The resonant modes of the structure were calculated by FDTD and it was found that we can easily manipulate the central wavelengths of the resonance transmission by adjusting the dimensions of the hollow while the outer dimensions of the ring are kept constant. To overcome the transmittance reduction of the hollow-core structure we proposed a decrease in the width of the ring MIM waveguide in the coupling region. The introduced miniaturized plasmonic filter is potentially a choice for designing all-optical integrated circuits for optical communication and optoelectronic circuits; especially when we have limitations on the outer size of the filter structure and we cannot achieve a longer resonant wavelength by conventional simple ring resonator filters.

Acknowledgment

The authors acknowledge the financial support from the Education & Research Institute for ICT, Iran (grant no. 500/3653).

References

[1] Bozhevolnyi S I 2008 Plasmonic nano-guides and circuits *Plasmonics and Metamaterials, OSA Technical Digest (CD)* Optical Society of America
[2] Ozbay E 2006 Plasmonics: merging photonics and electronics at nanoscale dimensions *Science* **311** 189–93
[3] Wang B and Wang G P 2004 Surface plasmon polariton propagation in nanoscale metal gap waveguides *Opt. Lett.* **29** 1992–4
[4] Veronis G and Fan S 2005 Bends and splitters in metal–dielectric–metal subwavelength plasmonic waveguides *Appl. Phys. Lett.* **87** 131102
[5] Han Z, Forsberg E and He S 2007 Surface plasmon Bragg gratings formed in metal–insulator–metal waveguides *IEEE Photon. Technol. Lett.* **19** 91–3
[6] Wang B and Wang G P 2005 Plasmon Bragg reflectors and nanocavities on flat metallic surfaces *Appl. Phys. Lett.* **87** 013107
[7] Liu J Q, Wang L L, He M D, Huang W Q, Wang D, Zou B S and Wen S 2008 A wide band gap plasmonic Bragg reflector *Opt. Express* **16** 4888–94
[8] Gramotev D K and Pile D F P 2004 Single-mode sub-wavelength waveguide with channel plasmon–polaritons in triangular *Appl. Phys. Lett.* **85** 6323–5
[9] Verhagen E, Dionne J A, Kuipers L, Atwater H A and Polman A 2008 Near-field visualization of strongly confined surface plasmon polaritons in metal–insulator–metal waveguides *Nano Lett.* **8** 2925–9
[10] Takahara J, Yamagishi S, Taki H, Morimoto A and Kobayashi T 1997 Guiding of a one-dimensional optical beam with nanometer diameter *Opt. Lett.* **22** 475–7
[11] Leosson K, Nikolajsen T, Boltasseva A and Bozhevolnyi S I 2006 Long-range surface plasmon polariton nanowire waveguides for device applications *Opt. Express* **14** 314–9
[12] Maier S A, Kik P G, Atwater H A, Meltzer S, Harel E, Koel B E and Requicha A G 2003 Local detection of electromagnetic energy transport below the diffraction limit in metal nanoparticle plasmon waveguides *Nature* **2** 229–32
[13] Quinten M, Leitner A, Krenn J R and Aussenegg F R 1998 Electromagnetic energy transport via linear chains of silver nanoparticles *Opt. Lett.* **23** 1331–3
[14] Maier S A, Kik P G and Atwater H A 2003 Optical pulse propagation in metal nanoparticle chain waveguides *Phys. Rev.* B **67** 205402
[15] Pile D F P and Gramotev D K 2004 Channel plasmon–polariton in a triangular groove on a metal surface *Opt. Lett.* **29** 1069–71
[16] Bozhevolnyi S I, Volkov V S, Devaux E and Ebbesen T W 2005 Channel plasmon–polariton guiding by subwavelength metal grooves *Phys. Rev. Lett.* **95** 046802

[17] Matsuzaki Y, Okamoto T, Haraguchi M, Fukui M and Nakagaki M 2008 Characteristics of gap plasmon waveguidewith stub structures *Opt. Express* **16** 16314–25
[18] Xiao S S, Liu L and Qiu M 2006 Resonator channel drop filters in a plasmon–polaritons metal *Opt. Express* **14** 2932–7
[19] Zhang Q, Huang X G, Lin X S, Tao J and Jin X P 2009 A subwavelength coupler-type MIM optical filter *Opt. Express* **17** 7549–54
[20] Hosseini A and Massoud Y 2007 Nanoscale surface plasmon based resonator using rectangular geometry *Appl. Phys. Lett.* **90** 181102
[21] Wang T B, Wen X W, Yin C P and Wang H Z 2009 The transmission characteristics of surface plasmon polaritons in ring resonator *Opt. Express* **17** 24096–101
[22] Yun B, Hu G and Cui Y 2010 Theoretical analysis of a nanoscale plasmonic filter based on a rectangular metal–insulator–metal waveguide *J. Phys. D: Appl. Phys.* **43** 385102
[23] Lu H, Liu X, Mao D, Wang L and Gong Y 2010 Tunable band-pass plasmonic waveguide filters with nanodisk resonators *Opt. Express* **18** 17922–7
[24] Maier S A 2007 *Plasmonics: Fundamentals and Applications* (Berlin: Springer)
[25] Dionne J A, Sweatlock L A, Atwater H A and Polman A 2006 Plasmon slot waveguides: towards chip-scale propagation with subwavelength-scale localization *Phys. Rev.* B **73** 035407
[26] Kim K Y, Cho Y K, Tae H-S and Lee J-H 2006 Light transmission along dispersive plasmonic gap and its subwavelength guidance characteristics *Opt. Express* **14** 320–30
[27] Rakić A D, DjuriŠić A B, Elazar J M and Majewski M L 1968 Optical properties of metallic films for vertical-cavity optoelectronic devices *Appl. Opt.* **37** 5271–83